JOURNAL OF GEOPHYSICAL RESEARCH, VOL. 89, NO. A3, PAGES 1667–1674, MARCH 1, 1984

Phase Measurements of Whistler Mode Signals From the Siple VLF Transmitter

E. W. PASCHAL AND R. A. HELLIWELL

Space, Telecommunications and Radioscience Laboratory, Stanford University

A digital signal processing program has been developed to measure the phases of coherent VLF signals from analog tape recordings made in the field. The program uses a constant frequency pilot tone recorded with the VLF data to correct tape speed errors and reconstruct the signal phases. We analyze several examples of whistler mode signals from the VLF transmitter at Siple Station, Antarctica, as received at Roberval, Quebec. Pulses with temporal growth show a relative phase advance with time, and thus a positive frequency offset from the transmitted signal, often from the beginning of the pulse. Amplitude beating is often seen toward the end of a pulse, sometimes with phase cycle-skipping as the emission becomes unlocked from the input signal. Current theories of wave-particle interaction are reviewed and found to explain some of the observed signal features, though no theory predicts the initial frequency offset of a growing pulse.

1. INTRODUCTION

Measurements of the spectral characteristics of whistler mode signals have been used for many years to study propagation and wave-particle interactions in the magnetosphere [e.g., *Park and Carpenter*, 1978; *Helliwell and Katsufrakis*, 1978]. However, with a few notable exceptions [*Dowden et al.*, 1978; *Rietveld et al.*, 1978; *Rietveld*, 1980], most studies have examined only the signal amplitudes as functions of frequency and time and have not considered the signal phases. There are two reasons for this. First, naturally occurring signals such as whistlers and chorus are complex, and their phase characteristics are less easily interpreted than their amplitude characteristics. Second, phase is more difficult to measure than amplitude, requiring special recording techniques and analysis apparatus. Yet if the signals studied are simple enough (such as phase-coherent signals from VLF transmitters) their phases, which contain information independent of their amplitudes, can add a new dimension to our understanding of magnetospheric phenomena. In this report we will briefly describe our technique for measuring the phase of whistler mode VLF transmitter signals and present some preliminary results and their implications for current models of wave-particle interaction.

2. ANALYSIS METHOD

One of the major problems in making phase measurements is to record the signals in the field in such a way that their phases can be reconstructed upon playback. Direct analog tape recording is the simplest and cheapest recording method but suffers from wow and flutter both during recording and reproduction. If tape speed errors are large enough, signal components may even be shifted in frequency outside the passbands of the filters used during analysis.

The wow and flutter problem can be overcome by inserting in the recorded data a constant frequency phase reference pilot tone. *Dowden et al.* [1978] have developed such a technique by using analog signal processing. In their method, a frequency synthesizer is phase locked to the pilot tone and provides a reference signal at a desired data frequency. The data are filtered and mixed with this reference signal, and the difference is displayed as a "phasogram," which shows the relative data phase at that frequency versus time. Our method is similar, except that we use digital rather than analog signal processing.

The analysis of VLF data with our method proceeds as follows. First, the analog data are played back and digitized. The FFT algorithm is used to calculate the discrete Fourier transform of successive overlapping blocks of data. The resulting spectral points in each transform are convolved with a short window function to improve the shape of the synthesized filters, widening their passbands and suppressing sidelobe responses. Next, the phase of the pilot tone is measured and used to calculate the actual time of the particular data block. The advance in pilot phase from the previous block is measured and provides the instantaneous pilot frequency, and thus the speed error at that moment.

Knowing the speed error, next we interpolate between spectral points in the transform to generate a new spectrum whose points correspond to the original data frequencies. Using linear interpolation between transform points to unshift the spectrum will change the shape of the synthesized filter passbands, and it is not immediately obvious that this is a useful technique. However, if there is sufficient overlap in the passbands of the transform filters (which depends on the window function), then the changes in filter shape from interpolation can be made as small as desired. For instance, we usually use the three-term minimum sidelobe window function given by *Nuttall* [1981], which gives the filters in the transform a 3-dB width about 1.6 times their spacing in frequency. With this window function the worst case change, which occurs when synthesizing a new spectral point midway between two points in the transform, amounts to a 1.1-dB decrease in filter center gain, a negligible change in 3-dB bandwidth, and a slight broadening of the filter skirts. Fortunately, interpolation has almost no effect on the phase response of the filters.

Finally, the phase of each spectral point in the speed-corrected spectrum is converted to a relative phase measurement by subtracting a phase of $2\pi ft$ radians, where f is the center frequency of the spectral filter and t is the time of

Paper number 3A1947.
0148-0227/84/003A-1947$05.00

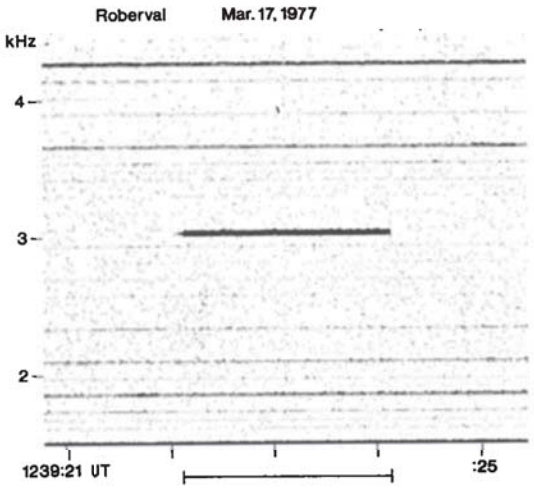

Fig. 1. Spectrogram of a 2-s pulse from Siple to Roberval at 3030 Hz. The pulse is constant in amplitude, showing neither temporal growth nor emission triggering.

the particular data block. These results are plotted, the transform of the next data block is taken, and so on. The resulting output for each spectral filter is a plot of the phase of the original VLF signal, filtered around the frequency f, with respect to the phase of a reference oscillator which has been running at exactly f Hz.

Interpretation of relative phase plots is straightforward. If the relative phase of the signal filtered at frequency f increases by, say, q revolutions per second, then we know that are the actual signal frequency was $f + q$ Hz. In this way we can make instantaneous frequency measurements of signal components more easily and accurately than from conventional amplitude versus frequency spectrograms. For example, *Rietveld* [1980] has used phase measurements of whistler precursors to measure their instantaneous initial frequency and found, contrary to the evidence of conventional spectrograms, that they did not start at the frequencies of power line harmonics but were several hertz away. We can also use phase analysis to observe more complex types of signal behavior, as will be illustrated in the data plots that follow.

3. Experimental Results

The following data illustrate typical features of whistler mode signals propagating along field lines near $L = 4.2$ from the Siple Station VLF transmitter to the conjugate point near Roberval, Quebec. We emphasize, however, that these examples have been selected for the simple behavior they portray. So while these examples are believed to be typical, they should not be construed as representing all the types of behavior that may be found, or even necessarily average behavior. In many cases where temporal amplification and triggering from transmitted signals occur, the phase and amplitude behavior of the received signals is much more complicated and difficult to interpret than in the following cases.

Linear Propagation

Figure 1 is a spectrogram of a 2-s pulse at 3030 Hz from Siple as received at Roberval. This pulse is typical of pulses that show little or no temporal growth received during times of good propagation. The bar below the spectrogram shows the duration of the transmitted pulse. Note that the received pulse is slightly longer, about 2.1 s, but weak during the first 0.1 s, owing to multi-path propagation.

Figure 2 is a plot of the log magnitude and relative phase of the 2-s pulse. The magnitude plot shows a slow rise in amplitude during the first 0.1 s, before the main part of the pulse, with two plateaus, indicating two additional paths of propagation. The data block used in this analysis was 80-ms long, with an effective windowed half-width of 33 ms, so the plateaus are somewhat smeared. The main part of the pulse is quite strong and relatively constant in amplitude, though toward the end it develops an 11-Hz ripple of about 2.5-dB peak to peak amplitude.

The phase plot in Figure 2 shows the phase of the received signal with respect to a synthesized oscillator running at exactly 3030 Hz. The phase plot is 5 revolutions (1800°) full scale. The phase of the received signal is relatively smooth, with small variations about 20° pp, decreases slowly with time, at about −0.15 revolution per s. This indicates that the received wave was 0.15 Hz below the center frequency of the filter, or at 3029.85 Hz. Similar drifts were observed on other pulses shortly before and after this one. 0.15 Hz is typical of the larger drifts seen with nongroving signals.

McNeill [1967] reported relative frequency changes averaging 6×10^{-6} for whistler mode signals from NPG at 18.6 kHz, which he attributed to drift of the magnetospheric path with a possible minor contribution from ionospheric electron density changes. The 0.15-Hz drift here is a relative frequency change of 50×10^{-6} but is consistent with his results considering the longer path at higher magnetic latitude in this case. Thus the phase drift is probably due to path length changes caused by duct drift. Given signals of sufficiently long duration, it is possible to use phase analysis to measure long-term duct motion much as is done with conventional whistler nose-frequency analysis but without the need for whistlers. *Rietveld et al.* [1978] have

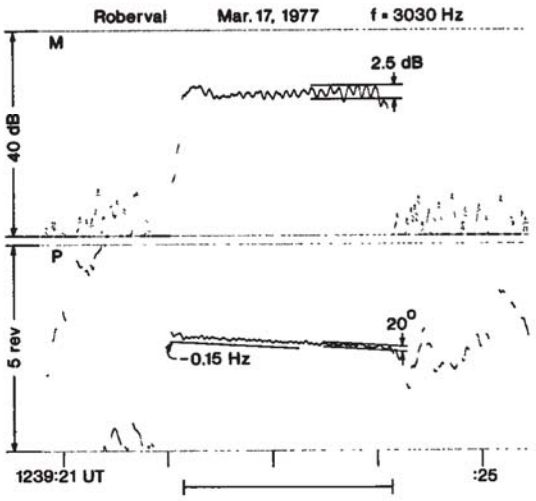

Fig. 2. Plot of the magnitude M and phase P of the pulse in Figure 1. Two plateaus on the leading edge of the magnitude plot indicate two additional paths of propagation. Pulsations in amplitude develop toward the end of the pulse. The phase plot shows that the received frequency is 0.15 Hz below the transmitted frequency due to an increase in path length during the pulse.

used the "phasogram" method to measure such drift, and report correlations between duct motion at $L = 3.8$ and Pc 3 micropulsations. However, the use of phase analysis to observe duct motion on a regular basis will be hampered by the need for stable signals that do not show temporal growth, since the phase changes due to such growth can completely mask the smaller changes due to path drift.

The amplitude ripple that develops toward the end of the pulse is similar to the pulsation phenomenon reported by *Bell and Helliwell* [1971] and may be caused by wave-particle interaction. It is possible, of course, that the ripple is caused by beating between signals propagating along different paths drifting at different rates. To generate an 11-Hz ripple of 2.5 dB pp we would require two signals, one about 17 dB lower in amplitude and 11 Hz offset in frequency from the other. We would also expect to see beats in the phase plot about 16° pp. While the first multi-path signal that arrives (the first small plateau on the rising edge of the magnitude plot) is about 17 dB below the main part of the pulse, and the small variations in the phase plot are about 20° pp, there is no clear correlation between the phase ripples and the amplitude ripples. Furthermore, the amplitude ripples seem to grow with time, whereas beating should produce ripples that are constant with time. It is also difficult to imagine that the first signal could have been offset by as much as 11 Hz from the main signal. So while we cannot rule out multi-path beating as the cause of the amplitude ripples, it seems unlikely.

Temporal Growth

Figure 3 shows the spectrogram of a 1-s pulse at 2000 Hz. The bar below the spectrogram shows the duration of the transmitted pulse and has been shifted in time according to the propagation delay measured from other signals received at this time. During the first few tenths of a second the pulse is relatively constant in frequency but shows growth in amplitude. After about 0.7 s the pulse broadens in frequency and gives rise to an emission which continues for about 2 s.

Figure 4 is a magnitude-phase plot of the pulse in Figure 3. In this case a filter bandwidth of 160 Hz was used, with a corresponding data block length of 10 ms, in order to improve the time resolution of the pulse and include any wide-band signals near the transmitted frequency. The magnitude plot shows the pulse growing at a rate of 36 dB/s up to the time when the emission appears on the spectrogram. Near the end of the growth phase the magnitude plot shows ripples in amplitude at a 35-Hz rate. The phase plot shows a relative phase advance with time throughout. Even at the beginning of the pulse the phase advance indicates that the received signal is about 1.1 Hz above the frequency of the transmitted signal, a much greater change in frequency than would be expected from path drift. Near the end of the pulse, when the emission starts to separate from the input signal, the instantaneous frequency is about 63 Hz above the input frequency. The discontinuity labeled "tracker error" is due to a spheric that caused the pilot tone phase tracker in the analysis program to jump 1 cycle in phase for the 10-kHz pilot tone recorded in this case, or 0.2 revolutions in phase at 2000 Hz. The phase plot should be continuous at this point, of course.

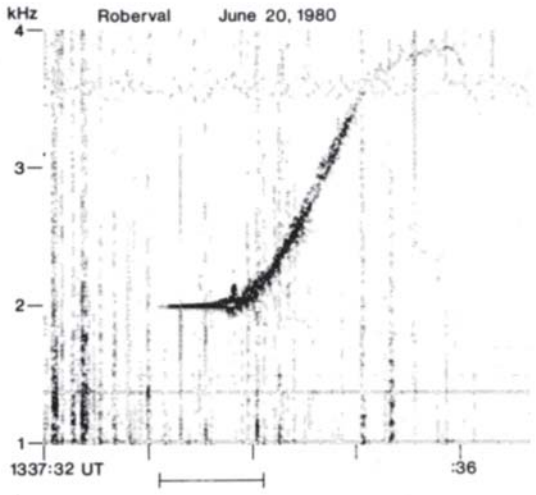

Fig. 3. Spectrogram of a 1-s pulse at 2000 Hz showing growth in amplitude with time and the generation of an emission.

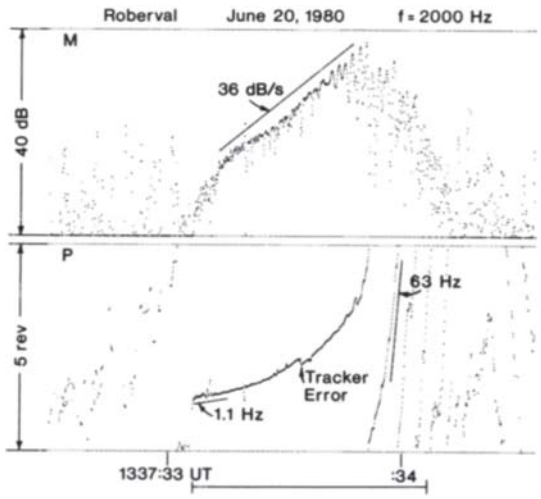

Fig. 4. Magnitude and phase plot of the pulse in Figure 3. The growth rate is 36 dB/s before saturation. The phase plot shows that the pulse is offset by +1.1 Hz from the transmitted frequency at the start, and the frequency offset increases with time. When the emission starts to separate, the received signal is 63 Hz above the transmitted frequency.

Figure 5 shows another 1-s pulse. The pulse of interest is identified by the bar under the spectrogram. At this time the transmitter was sending a complicated format containing various pulses at other frequencies and frequency ramps, some of which can also be seen. The pulse of interest is relatively constant in frequency and shows growth for the first 0.8 s. At that time, the pulse broadens in frequency and generates an emission that rises in frequency and later becomes entrained by a frequency ramp sent just after the pulse. This record also shows rather strong local power line interference.

Figure 6 shows the magnitude and phase of this pulse. The pulse amplitude grows at 37 dB/s and then saturates. The phase plot shows a nearly constant rate of phase advance with time, with the received pulse being about 3.1 Hz above the transmitted frequency. Note that this frequency offset continues even after the pulse amplitude has saturated, and up to the time when the emission separates. Other pulses seen near this time have exhibited frequency offsets from 0 to +6 Hz, growth rates from 0 to 60 dB/s, and saturation amplitudes over a 31-dB range. However, there

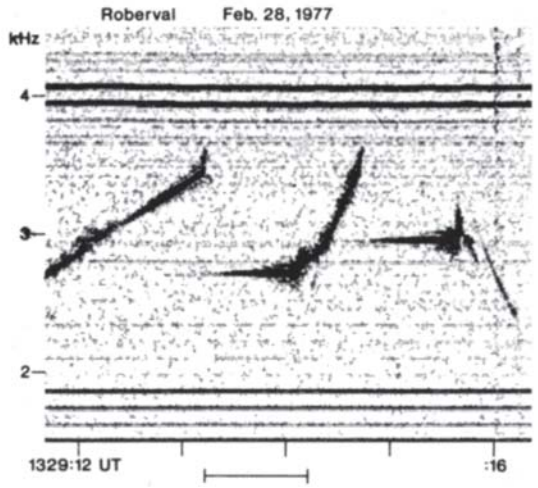

Fig. 5. Spectrogram of a series of ramping-frequency and constant-frequency pulses. The 1-s pulse of interest at 2710 Hz is indicated by the bar under the plot. The pulse shows growth and the generation of an emission that is entrained by a following ramp.

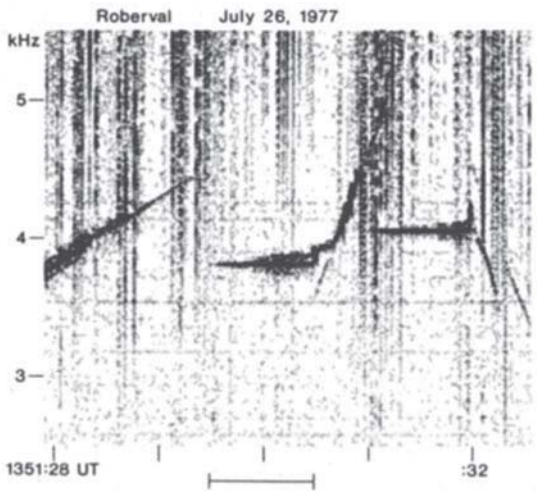

Fig. 7. Spectrogram of a transmission similar to that in Figure 5. The 1-s pulse at 3810 Hz again shows growth and an emission that becomes entrained by a following ramp.

seems to be little correlation between the frequency offset, growth rate, or saturation amplitude of different pulses. Pulses always show a positive frequency offset when growth occurs, and we have never seen more than a momentary phase decrease on any growing pulse. Pulses without temporal growth usually show constant relative phase with time, other than the much slower phase changes associated with path drift.

Figure 7 shows another 1-s pulse, with a transmitter format similar to that in Figure 5. In this case, the emission frequency seems to be relatively constant, about 100 Hz above the frequency of the transmitted pulse, up to the time of entrainment by the following ramp. Figure 8 shows the magnitude and phase of this pulse. The growth rate here is about 27 dB/s. The phase plot shows a frequency offset of about 2.4 Hz for the first half of the pulse, though with a slight temporary phase decrease about 0.3 s from the start. The interesting feature in this plot is the behavior of the phase near the end of the pulse. The phase begins to oscillate with an amplitude of about 1/2 revolution and a period around 20 ms and then periodically jumps by 1 revolution and oscillates a few more times. One or two similar phase jumps may also be seen at the end of the pulse in Figure 6. After the end of the transmitted pulse the emission is seen to be about 120 Hz above the input frequency.

Figure 9 shows the magnitude and phase of the end of this pulse on an expanded time scale. In this plot the magnitude scale is linear and the phase is shown 1 revolution full scale. The transmitted pulse is represented by a bar under the graph, and the phase jumps are indicated by arrows. Between the phase jumps, the phase oscillates in an irregular fashion, but the trend during each interval of oscillation is to maintain a frequency offset of 2.4 Hz, the same as the offset during the growth phase. When the phase jumps occur, the phase seems to change at about the same rate as after the end of the pulse; that is, with the emission

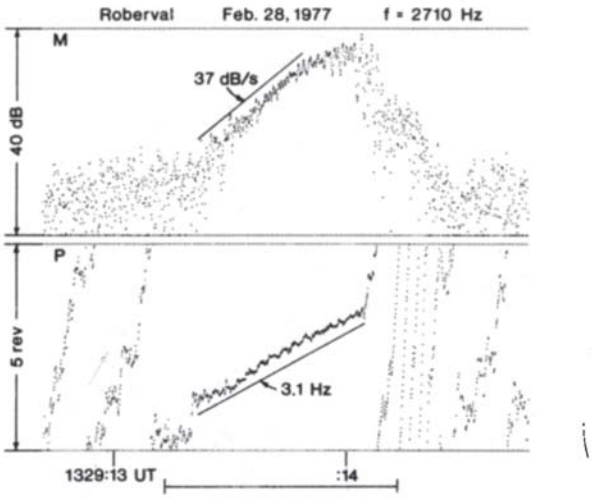

Fig. 6. Magnitude and phase plot of the pulse in Figure 5. The growth rate is 37 dB/s before saturation. The received pulse is 3.1 Hz above the transmitted frequency throughout the growth phase.

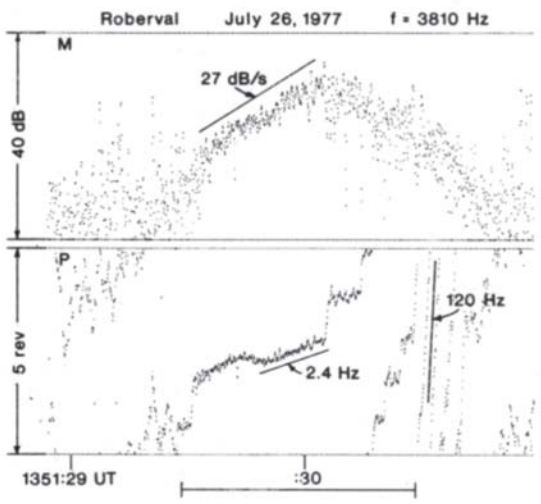

Fig. 8. Magnitude and phase plot of the pulse in Figure 7. The average frequency offset is 2.4 Hz during most of the growth phase. Note the periodic jumps in phase of 1 revolution after saturation but before the end of the input signal.

offset of 120 Hz. However, after each phase jump the signal phase is slightly below that expected by extrapolating the phase drift (2.4 Hz) from the previous interval, with the result that the overall phase change (excepting the jumps) is close to zero for the last 0.4 s or close to the phase of the input signal. It is as if the incipient emission is phase locked to the input signal, though with some phase variations, but periodically becomes unlocked, jumps ahead one cycle, and becomes locked again. And while locked, signal frequency is offset as in the earlier growth phase.

However, the real situation must be more complicated than this simple description suggests. For example, in Figure 9 we see that the signal shows relatively evenly spaced ripples in amplitude at about a 60-Hz rate. Also, there is only a weak correlation between the amplitude ripples and the phase ripples, with amplitude minima tending to coincide with phase peaks (though not always). And there seem to be many more phase ripples than amplitude ripples.

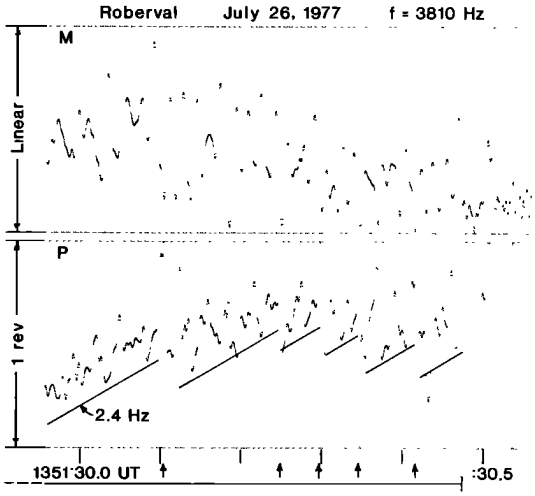

Fig. 9. Expanded magnitude and phase plot of the end of the pulse in Figure 7. The phase jumps are shown by arrows under the plot. During the intervals between phase jumps the frequency offset averages about 2.4 Hz, the same as during the growth phase. However, the phase from one interval to the next remains fairly constant, indicating that the output signal is still phase locked to the input.

4. Comparison with Current Theories

Many studies have been made of possible wave-particle interaction mechanisms to explain the occurrence of wave amplification and emission generation (see *Matsumoto* [1979] for a review and *Helliwell and Inan* [1982]). The most promising models have been based on doppler-shifted cyclotron resonance between waves and electrons. Unfortunately, the problem is complex, and each author has had to make various simplifying assumptions to make it tractable, with the result that no study has yet explained all the observed phenomena in a completely satisfactory manner. Indeed, the more complex models, which might be expected to give more realistic answers, are so complex that the physical processes underlying the observations are often obscured. Most treatments attempt to explain the overall frequency characteristics of amplification and emission, but only those by *Nunn* [1974], *Dowden et al.* [1978], and *Helliwell and Inan* [1982] make any particular predictions about phase behavior, probably because of the paucity of experimental phase data for comparison. We will concentrate on these three treatments and compare them with the data.

Nunn [1974] analyzes the effects of a transmitted pulse at half the equatorial gyrofrequency moving through a wave-particle interaction region near the equator in an inhomogeneous medium. The interaction is assumed to be narrow band, so that the particles remain in resonance with the wave. (Strongly trapped particles whose phase excursions are small seem to play the dominant role in this model.) Nunn integrates the fields produced by three streams of resonant particles at different pitch angles and finds the amplitude and phase of the total field as the pulse passes through the interaction region. Nunn's model is unable to account for amplitude saturation, except in a rather artificial way.

Nunn's model shows amplitude growth during passage of the pulse, with an initial slow phase decrease of up to 10° or 20° followed by a steady phase advance at an increasing rate (increasing positive frequency offset). After passage of the input pulse, the emission phase continues to advance smoothly at an increasing rate until the amplitude begins to pulsate as beating occurs between the main wave and a stimulated upper sideband. As Nunn points out, the model ceases to be valid at this point. Depending on the location of the interaction region with respect to the equator, Nunn's model can generate rising or falling tones (the latter after a short initial rise in frequency) in accordance with *Helliwell* [1967].

Nunn's model is quite successful in predicting the wave growth and general phase advance that is seen during the transmission of a relatively short pulse. His finding of a slow phase decrease at the very beginning of the pulse does not seem to occur very often, if at all, in the real data. Typical behavior at the beginning of a pulse seems more like that shown in Figure 4 where the signal phase advances monotonically, and where the received frequency is often offset from the transmitted signal from the start. However, the initial phase decrease may not be an important feature of the model, and may disappear with a different choice of parameters. Unfortunately, Nunn's model cannot be used later in time to explain the beating between the emission and the amplified signal.

Dowden et al. [1978] expand on Nunn's work and develop a feedback model containing two interaction regions, one trapping particles resonant with the input wave, and a second trapping particles resonant with the incipient emission. Since they use the resonant currents derived from Nunn's model they are again unable to account for saturation phenomena. However, by using separate interaction regions thay are better able to account for the interaction of the amplified wave and the incipient emission. They present phase measurements of amplified transmitter signals at 6.6 kHz, and use the feedback model to explain their observations. Their most important discovery is the "N event," a sudden decrease in phase of the output wave caused by beating between the amplified signal and the "embryo" emission, which tends to decrease the frequency of the output signal and keep the embryo emission entrained by the input wave.

The phase locking and periodic unlocking seen at the end of the transmitted pulse in Figure 9 seems to be similar to a series of N events. However, in our case the signal seems to be mostly locked to the input with periodic spasms of un-

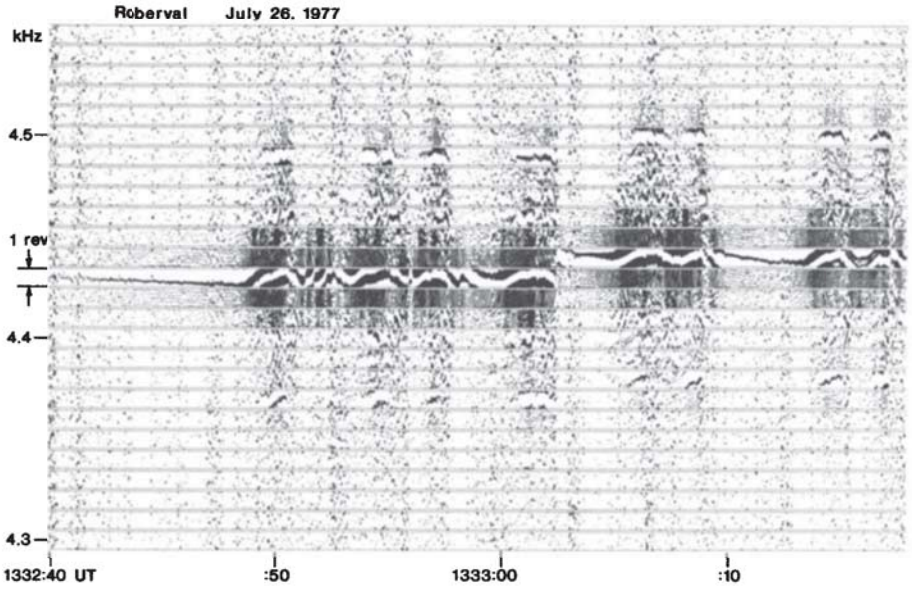

Fig. 10. Combined magnitude-phase plot of a cw signal starting at 4430 Hz. The outputs of 26 spectral filters from 4300 to 4500 Hz are shown. The filters are spaced every 10 Hz, and each has a bandwidth of 20 Hz. Trace width is proportional to signal magnitude, and trace position to signal phase, 1 revolution full scale. Note the growth and phase instability starting at 1332:48, and the subsequent generation of bursts of coherent sidebands 60 Hz from the amplified cw signal. At 1333:02 the transmitter frequency is increased by 10 Hz to 4440 Hz. The sidebands also increase by 10 Hz to remain 60 Hz away from the input signal.

locking, whereas in Dowden's analysis the signal is mostly the emission with periodic incidents of relocking to the input. But the difference here is probably one of emphasis, and the phenomenon we have observed is probably the same as the N event. Dowden's theory seems to explain these quite well, at least in a qualitative way. However, Dowden et al. have had to make some simplifying assumptions about the interaction of the input wave, the temporally amplified wave, and the emission; and as we have seen above the real situation is quite complicated.

Helliwell and Inan [1982] describe a model in which the distributed interaction is simulated by two lumped elements: a buncher where the output wave field organizes the phases of entering electrons, and a radiator where the electrons radiate and add to the input wave field. They derive the magnitude and phase of the system loop gain by tracing the trajectories of a monochromatic stream of 12 electrons with a single pitch angle, but equally spaced initial phases, through a wave field and calculating the currents produced. Large particle phase changes are allowed during the interaction, and the system loop gain shows the effect of saturation at large amplitudes. They then use the loop gain derived to calculate the output wave amplitude and phase for various input waves as a function of time. This is an appealingly simple model, though it is still a simplification of the actual mechanism since the loop parameters are determined for a monochromatic stream of particles and a single wave frequency, and since the feedback interaction occurs at two discrete points rather than being distributed in space.

Helliwell and Inan's model predicts amplitude growth and phase advance with time during the initial part of the transmitted pulse. They show the frequency offset of the output wave growing with time, but starting from the transmitted frequency and do not predict the initial offset seen in Figure 4. After a sufficient time the output amplitude will reach saturation and they predict that the loop phase shift may then become negative, with the result that the output signal phase begins to retard. This does not seem to be the case, at least in the data studied so far.

In conclusion, these three studies succeed to varying degrees in explaining in a qualitative way the phenomena observed. They all explain the general phase advance seen during the growth of a transmitted pulse, though (at least for some initial conditions) Nunn's model predicts a small phase decrease that does not seem to be observed. Dowden et al. explain the simpler features of the input-emission beating and the phase jumps that are observed just before the emission separates from the input signal. Helliwell and Inan include the effects of wave saturation, though with phase effects that seem to disagree with the observations. However, all assume that the output wave starts at the frequency of the input, and no model explains the apparent initial frequency offset that sometimes appears.

5. Other Phenomena

Figure 10 is the magnitude-phase spectrogram of a continuous wave transmission from Siple. This record was previously studied by *Park* [1981], but without the benefit of phase measurements. In Figure 10 the outputs of several analysis filters are presented simultaneously. The width of the trace for each filter output is proportional to the output magnitude, and the vertical position of each trace is proportional to the output phase, with a full scale deflection representing 1 revolution (360°). The output filters are spaced every 10 Hz, and each has a 3-dB bandwidth of about 20 Hz. Leakage of the signal at one frequency into adjacent filters generates the chevron pattern seen.

At the beginning of the plot the Siple transmitter was sending a cw signal of constant power at 4430 Hz. The received signal is weak but relatively constant in phase, with a slow phase decrease typical of path drift. At about 1332:48

the signal begins to grow and the relative phase advances. After 2 s the phase has advanced about one revolution and it levels off. At this time two sidebands appear, 60 Hz above and below the amplified transmitter signal, or carrier. They last about 1.5 s, disappear, and the carrier phase begins to retard. The cycle of phase advance, sidebands, and phase decrease repeats every few seconds. At 1333:02 the transmitter frequency is increased by 10 Hz to 4440 Hz. Notice that the sideband frequencies also increase, remaining 60 Hz above and below the carrier. This process was observed to continue for some minutes, with the sidebands always changing along with the transmitted frequency. The amplitudes of the carrier and the sidebands were well correlated with the carrier phase, with carrier amplitude a maximum when the phase was advancing, and sideband amplitude a maximum when the phase was peaking. The two sidebands were not always equal in amplitude, however, with the upper sideband being usually stronger. In some cases only the upper sideband could be seen. By phase tracking on the carrier we have determined that the frequency offset of the sidebands is very close to 60 Hz, probably within 0.1 Hz. There may also be weaker sidebands around 30 Hz but the analysis filters are a bit too wide to be sure of this.

The sidebands cannot be power line radiation amplified separately from the transmitter signal, since their frequency changes with the transmitter frequency, and since they seem to be phase-locked to the amplified input signal. The transmitter used in this experiment was the older Zeus unit, a modified Navy pulse-switching transmitter, and the level of spurious sidebands in the transmitted signal is quite low, with 60-Hz modulation down by at least 40 dB, and more probably 60 dB, from the carrier. So the sidebands seem unlikely to be independently amplified spurious emissions from the transmitter. The transmitter power supply did have significant ripple at 360 Hz, which would generate sidebands offset 360 Hz from the carrier and only 20 to 30 dB lower in power, but these are not seen. Of course, they may be too low in level or too removed in frequency to be amplified at this time, since magnetospheric amplification is often a narrowband phenomenon. We have examined several other cases of similar cw transmission and often see signal growth and sideband noise, but usually 20 to 40 Hz from the carrier and seemingly incoherent. This is the only case where such coherent sidebands, and at such an odd frequency, have been seen.

We have no ready explanation for this case. However, it is conceivable that beats between amplified power line radiation harmonics could temporarily trap longitudinally resonant electrons as in the *Park and Helliwell* [1977] explanation of whistler precursors, causing a periodic density bunching of these electrons. This bunching might then cause cyclotron-resonant waves to be modulated at the 60-Hz beat frequency.

6. SUMMARY

We have shown how analog VLF recordings from field stations may be analyzed to study the phases of coherent signals as well as their amplitudes. Using a phase-reference pilot tone recorded with the data, frequency shifts due to tape wow and flutter can be corrected and the phases of signal components can be reconstructed and measured. Phase measurements open up a new dimension in the study of magnetospheric signal propagation and add new insights to our understanding of the interaction of whistler mode waves and particles. Instantaneous frequency measurements that are difficult or impossible to make with conventional spectrum analysis are made easily and accurately when phase information is available. These include the measurement of doppler-shifted wave frequency due to path drift, frequency offsets during wave amplification, and the frequency of sideband noise. Phase measurements during amplitude pulsations and emission triggering may help elucidate these processes.

The observed phase behavior of signals during temporal growth and emission generation is seen to be a major constraint in the selection of theories to explain wave-particle interaction. Up to the present time, few theories have made any predictions about signal phase behavior. Of those that have, some predictions agree reasonably well with the observations, but many do not. No current theory predicts all of the phase features observed, in particular the initial positive frequency offset of a growing pulse. We hope that the availability of phase observations will stimulate the development of new theories and bring us closer to an understanding of the mechanism of wave-particle interactions in the magnetosphere.

Acknowledgments. We thank J. Katsufrakis for his efforts as supervisor of the Stanford VLF field programs and W. Trabucco for his contributions to the VLF transmitting system at Siple. We are grateful to the field personnel responsible for data acquisition, and to our other colleagues for their interest and support. Typescript was prepared by G. Walker. This research was supported by the Division of Polar Programs of the National Science Foundation under grants DPP76-15678, 80-22282, and 80-22540.

The Editor thanks David Nunn and R. L. Dowden for their assistance in evaluating this paper.

REFERENCES

Bell, T. F., and R. A. Helliwell, Pulsation phenomena observed in long-duration VLF whistler mode signals, *J. Geophys. Res., 76*, 8414–8419, 1971.

Dowden, R. L., A. D. McKay, L. E. S. Amon, H. C. Koons, and M. H. Dazey, Linear and nonlinear amplification in the magnetosphere during a 6.6-kHz transmission, *J. Geophys. Res., 83*, 169–181, 1978.

Helliwell, R. A., A theory of discrete VLF emissions from the magnetosphere, *J. Geophys. Res., 72*, 4773–4790, 1967.

Helliwell, R. A., and U. S. Inan, VLF wave growth and discrete emission triggering in the magnetosphere: A feedback model, *J. Geophys. Res., 87*, 3537–3550, 1982.

Helliwell, R. A., and J. P. Katsufrakis, Controlled wave-particle interaction experiments, in *Upper Atmosphere Research in Antarctica, Antarctic Res. Ser.* Vol. 29, edited by L. J. Lanzerotti and C. G. Park, pp. 100–129, AGU, Washington, D. C., 1978.

Matsumoto, H., Nonlinear whistler mode interaction and triggered emissions in the magnetosphere: A review, in *Wave Instabilities in Space Plasmas*, edited by P. J. Palmadesso and K. Papadopoulos, pp. 163–190, D. Reidel, Hingham, Mass., 1979.

McNeill, F. A., Frequency shifts on whistler mode signals from a stabilized VLF transmitter, *Radio Sci., 2*, 589–594, 1967.

Nunn, D., A self-consistent theory of triggered VLF emissions, *Planet. Space Sci., 22*, 349–378, 1974.

Nuttall, A. H., Some windows with very good sidelobe behavior, *IEEE Trans. Acoust. Speech Signal Process., ASSP-29*, 84–91, 1981.

Park, C. G., Generation of whistler mode sidebands in the magnetosphere, *J. Geophys. Res., 86*, 2286–2294, 1981.

Park, C. G., and D. L. Carpenter, Very low frequency radio

waves in the magnetosphere, in *Upper Atmosphere Research in Antarctica, Antarctic Res. Ser.* Vol. 29, edited by L. J. Lanzerotti and C. G. Park, pp. 72–99, AGU, Washington, D. C., 1978.

Park, C. G., and R. A. Helliwell, Whistler precursors: A possible catalytic role of power line radiation, *J. Geophys, Res., 82,* 3634–3642, 1977.

Rietveld, M. T., Monochromatic precursor starts, *J. Geophys. Res., 85,* 2027–2036, 1980.

Rietveld, M. T., R. L. Dowden, and L. E. S. Amon, Micropulsations observed by whistler mode transmissions, *Nature, 276,* 165–167, 1978.

E. W. Paschal and R. A. Helliwell, Space, Telecommunications and Radioscience Laboratory, Stanford University, Stanford, CA 94305.

(Received August 12, 1983;
revised December 12, 1983;
accepted December 13, 1983.)